Handbook of
ELECTROCHEMICAL NANOTECHNOLOGY

Volume 1
Nanomaterials

Edited by

Yuehe Lin
Pacific Northwest National Laboratory, Richland, Washington, USA

Hari Singh Nalwa
Nanomax Technologies, Los Angeles, California, USA

AMERICAN SCIENTIFIC PUBLISHERS
25650 Lewis Way
Stevenson Ranch, California 91381-1439, USA

AMERICAN SCIENTIFIC PUBLISHERS
25650 Lewis Way, Stevenson Ranch, California 91381-1439, USA
Tel.: (661) 254-0807
Fax: (661) 254-1207
E-mail: order@aspbs.com
URL: http://www.aspbs.com

Handbook of Electrochemical Nanotechnology edited by Yuehe Lin and Hari Singh Nalwa

The images for the cover of this book was provided by Dr. Yuehe Lin from Pacific Northwest National Laboratory, USA.

This book is printed on acid-free paper. ♾

Library of Congress Control Number: 2005927979

International Standard Book Number: 1-58883-039-X (2-Volume Set)
International Standard Book Number: 1-58883-121-3 (Volume 1)
International Standard Book Number: 1-58883-122-1 (Volume 2)

PRINTED IN THE UNITED STATES OF AMERICA
10 9 8 7 6 5 4 3 2 1

CHAPTER 4

Templated Ensembles of Nanoelectrodes

Ligia M. Moretto[1], Stefania Panero[2], Bruno Scrosati[2], Paolo Ugo[1]

[1] *Department of Physical Chemistry, University of Venice, Santa Marta 2137, 30123 Venice, Italy*
[2] *Department of Chemistry, University La Sapienza, 00185 Rome, Italy*

CONTENTS

1. INTRODUCTION

The synthesis of new nanostructured materials and the study of their properties (electrochemical, catalytical, and optical) compared to those of macroscopic samples of the same materials are attracting increasing interest in modern chemical science. The transition between bulk and molecular scales often leads to dramatic changes in the properties of a material, which can be interesting for the practical applications in a variety of areas, including chemistry, physics, electronics, optics, materials, and biomedical science [1–4]. This trend includes the preparation, characterization, and electrochemical applications of electrodes with critical dimensions in the nanometer range. Among other more complex and expensive procedures, the preparation of nanoelectrode using nanoporous membranes as templates distinguishes itself for its simplicity and wide applicability.

First attempts in such a direction started at the end of 1980s in Charles Martin's laboratory [5, 6], shortly followed by Uosaki and co-workers [7], who proposed the new idea of using preformed microporous membranes to build specially featured electrodes inside the pores of the membrane, so obtaining an integrated membrane-nanoelectrode device. These nanostructured electrodes showed quickly to be very useful for a variety of specialized functions spanning from chemical analyses and sensing [8] to photoelectrochemistry [9] and electrochemical energy storage [10, 11]. The first

ISBN: 1-58883-121-3

Handbook of Electrochemical Nanotechnology
Edited by Yuehe Lin and Hari Singh Nalwa
Volume 1: Pages: 87–105

prototype nanoelectrode ensemble (NEE) was built using alumina microporous membrane as template [5–7], which was then matched by track-etched polymeric membranes [2, 12] commercially available as ultrafiltration membranes (for sophisticated biological separations). All these membranes contain monodispersed pores of very small diameter; the pore diameter determines the nanoelectrode diameters and the pore density controls the distance between the nanoelectrode elements. Since the thickness of the templating membrane is usually much larger than the pore diameter, the obtained nanostructures are characterized by high aspect ratios (that is, the length/diameter ratio), which can be as high as 600 or more. Other approaches are based on exploiting as nanoelectrodes the defects generated in a self-assembled monolayer [13–16]. Recently, metal nanostructures have been obtained also using as templates the pores created by self-assembly of block copolymers under the influence of applied electric fields and high temperatures [17, 18]. For a recent review on self-assembly and nanofabrication in polymer matrices see Ref. [19]; those interested also in other methods for the fabrication of nanoelectrodes and arrays are addressed to a recent review by Arrigan [20].

The use of preformed microporous membranes as template for the synthesis of nanomaterials was somehow revolutionary, since it made accessible to almost any laboratory a simple but effective procedure for the easy preparation of nanomaterials of interest not only to the electrochemist but to all material scientists [21]. What is needed for the membrane-based synthesis of nanomaterials is, in fact, a very simple apparatus, such as an apparatus for metal deposition and basic electrochemical instrumentation.

Historically, fundamentals of template synthesis in nanoporous membranes were introduced by Possin [22] and refined by Williams and Giordano [23], who prepared different metallic nanowires with diameters as small as 10 nm within the pores of etched nuclear damage tracks in mica. The technique refined progressively with time, up to achieving the preparation of very sophisticated nanostructures, such as conically shaped nanoelectrodes with controlled vertex angle, obtained very recently by finely tuning the etching of the pores in the membrane [24, 25].

Templating membranes can be used to produce nanostructured electrode systems not only via template metal deposition, but also by use of other methods such as sol–gel [26–28] or chemical vapor deposition [26, 29]. This chapter will examine specifically the preparation, characterization, and electrochemical application of ensembles of nanodisc and nanofiber electrodes obtained by using micro- and nanoporous membranes as templates, together with their applications to electroanalytical and energy storage purposes.

2. TEMPLATING MEMBRANES

2.1. Comparison Between Templating Membranes

There are two main types of microporous membranes available for the template deposition of metal nanowires and related nanostructures: track-etched polymers and microporous alumina membranes. Details on the preparation and relevant characteristics of the two kinds of membranes are given below with a preliminary comparison of the main features being introduced here. Both types of membranes are commercially available, and special geometries can be obtained on request to the producers; for the case of the alumina membrane, note that they can be homemade in dedicated laboratories.

The main morphological difference between alumina and track-etched polymer membranes is that the alumina membranes, which are prepared by controlled anodization of aluminium [30, 31], are characterized by very high pore densities, so that the ratio between the pore area and the overall geometric area is a number not much smaller than unity (see Fig. 1(a)). On the contrary, as shown in Figure 1(b), track-etched polymeric membranes are indeed characterized by much smaller pore densities. They are prepared by irradiation of the polymer foil with nuclear fission fragments of heavy elements such as californium or uranium or by ion beams from accelerators. The tracked zone is then removed by a chemical etching agent, typically a solution of a strong alkali. The chemical etching determines the pore size and shape [32–34], while the time of tracking determines the pore density [32, 35]. Polymeric materials most widely used for preparing track-etched porous

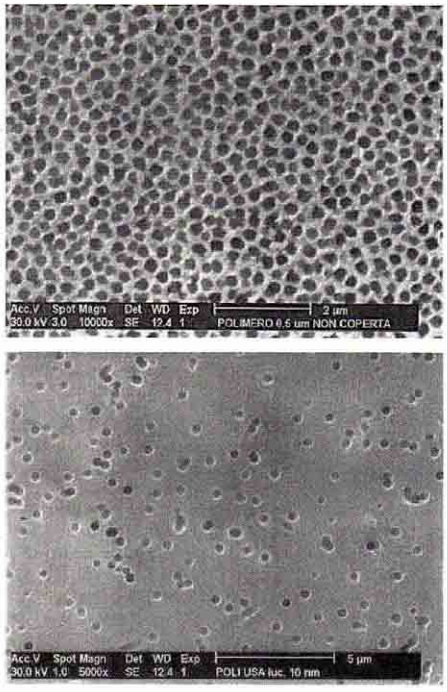

Figure 1. SEM images of commercial microporous membrane with pores of 200 nm diameter: (a) alumina; (b) track-etched polycarbonate.

membranes are polycarbonate, polyethylene terephthalate, and polyimide [32].

Advantageous characteristics of the track-etched membranes over porous alumina films are their flexibility (alumina films are brittle) and their smooth surfaces. A problem with track-etched membranes is that the pores created by fission fragment tracks are not always parallel to each other (or even perpendicular to the membrane surface), and pore positions are randomly distributed, unless special control procedure are applied [36]. On the other hand, the pores in the alumina membranes can be branched on one side of the membrane [37]. Both kind of membranes can be used for preparing NEEs; track-etched polymers are preferred when high distances between the nanoelectrode elements are required (as in case of analytical/sensing applications), while alumina membranes are the template of choice when high-density nanostructures represent the final goal (as in the case of high surface nanostructures for battery purposes). Also, the medium where the NEE should be used can determine the choice: alumina membranes resist to organic solvents where polymer membranes (in particular, polycarbonate membranes) can be dissolved; however, the former can be damaged by alkaline or acidic aqueous solutions.

2.2. Preparation of Microporous Alumina Membranes

Aluminium oxide films with regular pore distribution are formed when high-purity aluminium substrates is oxidized electrochemically in acidic electrolytes [30, 31]. The oxide film so produced consists of a uniform array of parallel alumina cells packed hexagonally, each containing a nearly cylindrical pore. The uniform diameter of the pores is a consequence of the equilibrium between the growth rate of the alumina and its dissolution into the acidic electrolyte. Repulsive forces between the pores due to the volume expansion causes such an hexagonal self-ordering of the pores [30]. By appropriate selection of the process conditions, films with pore diameters between <10 nm and 2 μm, pore density between 10^8 and 10^{11} pores/cm^2, and film thicknesses up to 200 μm can be obtained [38].

The oxidation is performed in a two-electrode cell, with the anode being a high purity (99.9 or even 99.99%) aluminium sheet. The metal surface is prepared by careful chemical or electrochemical polishing [39] or caustic etching. The cathode consists of a large plate of aluminium, lead, platinum, or stainless steel. The anodization can be performed potentiostatically or galvanostatically in a thermostatically controlled bath [30, 38, 40]. Potentials on the order of 10–160 V and current densities from 10 to 30 mA/cm^2 are usually applied; however, for high pore spacing, voltages as high as 700 V can be used [41]. The electrolyte is typically 15% sulfuric acid (15°C), 4% phosphoric acid (24°C), 2% oxalic acid (24°C), or 3% chromic acid (38°C) [30]; temperatures range from 38 to 0°C and even lower [31, 42, 43].

As shown in Table 1, the pore diameter of the membrane is proportional to the dc potential or to the current density applied. For a given voltage and temperature, the thickness of the porous aluminium oxide increases linearly, with the anodization time ranging from 0.1 to 10 μm. As well as the thickness, the pore spacing of the alumina film varies with the experimental conditions, particularly with applied potential and solution pH. For instance, for alumina films formed in 15% H_2SO_4 at 10°C, the pore density is 83×10^9 cm^{-2} or 30×10^9 cm^{-2} when the oxidizing potential is 15 and 30 V, respectively. It was also shown that pore densities decreases linearly with increasing pore diameters [39]. The effect of the applied anodizing voltage on pore density for films formed in 15% sulfuric acid at 10°C is presented in Table 2.

The growth of the oxide layer is such that it advances into the aluminium phase, with simultaneous formation and dissolution of the oxide occurring at the base of the pore. During the pore formation the aluminium anode material is never directly exposed to the solution, but it is always coated by a relatively thin nonporous oxide layer, called "barrier layer." Self-standing porous membranes are prepared from these films by removing the barrier layer to separate the unoxidized aluminium from the porous oxide layer [30, 44]. Different procedures can be used to this aim, the most widely used was developed by Furneaux et al. [41]; it consists of the so-called voltage reduction sequence (VRS). It entails stepwise reduction of the potential so that a progressive reduction of the pore diameter is produced at the bottom of the pore in correspondence of the lowering of the applied potential. After formation of this highly porous layer, the electrode is immersed into an acidic detachment solution (see Table 1). This results in the rapid dissolution of the interfacial oxide, which is faster where the smaller, branched pores give extended access (and reaction) to the surrounding Al_2O_3 layer. Under such conditions, the acid can finally access the substrate Al and, as a consequence, H_2 gas is evolved at the Al/Al_2O_3 interface. The evolving H_2 gas bubbles can be seen through the transparent alumina membrane; when these bubbles coalesce, detachment is complete. The Al electrode (with the detached alumina membrane still clinging to the surface) is then rinsed by immersion into water and dried in air. The membrane can be collected by sliding an index card between the alumina

Table 1. Conditions used for electrochemical preparation of the nanoporous alumina membranes and characteristics of the resulting membranes [39].

Applied potential (V)	Anodization time (h)	Electrolyte and concentration (% w/w)	Detaching acid concentration (% w/w)	Pore diameter (nm)
30	12	Oxalic acid (4%)	Phosphoric acid (25%)	52
20	4	Sulfuric acid (10%)	Sulfuric acid (25%)	32
15	6	Sulfuric acid (10%)	Sulfuric acid (25%)	22
10	10	Sulfuric acid (15%)	Sulfuric acid (25%)	16

Table 2. Pore density as a function of the applied anodizing voltage for films formed in 15% sulfuric acid at 10°C [30].

Anodizing voltage (V)	Pore density $\times 10^9$ cm^{-2}
15	83
20	56
30	30

and the substrate aluminium. The two faces of the detached alumina membrane are not equivalent: the face that was detached from the substrate Al surface contains remnants of the interfacial oxide layer, which can be removed by floating the membrane onto the surface of a 0.2 M KOH solution in ethylene glycol. This procedure tends to make both faces of the membrane essentially equivalent [39].

Another procedure to separate the porous film from the aluminium substrate is by immersing the anodized foil in a saturated aqueous $HgCl_2$ solution. This results in the amalgamation of aluminium along the Al_2O_3/Al interface and delamination of the oxide layer [45]. The impervious barrier layer in one side of the oxide film is removed (a process often referred to as a thinning process) by a dropwise chemical dissolution with 1 M NaOH, during which only the barrier layer side of the oxide film is exposed to the sodium hydroxide solution in order to prevent simultaneous dissolution of the entire oxide structure [45, 46]. Recently, an alternative procedure based on the so-called reverse bias potential was proposed by Mallouk and co-workers [47], in which there is a progressive reversing of the potential after the pore formation; both steps are performed in an acidic medium. The reverse bias potential is believed to increase the local pH concentration, promoting the dissolution of the oxide barrier layer.

2.3. Preparation of Track-Etched Polymer Membranes

Nanoporous polymeric membranes can be prepared by the track-etch method. This method entails tracking a film of solid material (polymer) with a beam of high-energy particles to create damage tracks in the film, which are then etched, forming monodisperse pores by exposition to an alkaline solution. The time the material is exposed to the tracking particles determines the number of tracks (and the following pores), while the etching time (as well as the composition of the etching solution) determines the size (and shape) of the pores.

Track-etched membranes ready for use are commercially available as filtration membranes, with pore diameters ranging from as small as 10 nm to as large as 10 μm. These membranes have high pore densities, for example, almost 10^9 pores cm^{-2} for the smallest pore diameter commercial membranes. Track but not etched nanoporous membranes are also commercially available, for example, from Osmonics (50 tracks/cm^2) or from Whatman, with higher pore density (10^7 tracks/cm^{-2}).

Different polymeric materials are used for the production of track-etched membranes: poly(ethylene terephthalate) (PET), polycarbonate (PC), polypropylene, polyvinylidene fluoride, polyimides, and CR-39 (allyl diglycol carbonate) [32]. The most widely used are probably PET and PC.

PC is the material used for preparing the majority of commercially available track-etched membranes. This polymer is characterized by a high sensitivity to tracking, it does not require UV sensitization, and it presents poor resistance to organic solvents and low wettability. Its hydrophilicity can be increased by impregnation with polyvinylpyrrolidone.

PET presents a high etch ratio, allowing the production of membranes with a wide range of pore diameters. Alkali solutions are used to develop the tracks. The membranes obtained are relatively hydrophilic, rather stable to acids and organic solvents, and biologically inert.

There are two basic methods of producing latent tracks in the polymer foils to be transformed into porous membranes [32]. The first method is based on the irradiation with fragments from the fission of heavy nuclei such as californium or uranium [48] in a nuclear reactor. Typical energy losses of the fission fragments are about 10 keV/nm. The fission fragments coming from a thin layer target have an almost isotropic angle distribution. To create an array of latent tracks penetrating the foil, a collimator is normally used.

The advantages of the tracking with fission fragment are

(a) good time stability of the particle flux,
(b) a nonparallel particle flux (enables the production of a high porosity and low percent of pore channels), and
(c) relatively low cost.

The limitations of the method are

(a) contamination of the tracked foil with radioactive products ("cooling" of the irradiated material is needed, which usually takes a few months),
(b) limited thickness of the membrane to be tracked,
(c) limited possibilities of controlling the angle distribution of the tracks, and
(d) production of tracks with different etching properties by fragments of different masses and energies.

The second method is based on the use of ion beams in accelerators. The intensity of the ion beam should be at least 10^{11} s^{-1}. To irradiate large areas, a scanning beam is normally used.

The advantages of the ion beam accelerator tracking method are

(a) there is no radioactive contamination of the material when the ion energy is below the Coulomb barrier,
(b) the identity of the bombarding particles gives tracks with the same etching properties,
(c) a large range of high energy particles makes possible the tracking of thicker membranes,
(d) there are better conditions for producing high-density ($>10^9$ cm^2) track arrays,
(e) particles heavier than fission fragments can be used (^{238}U for example), and
(f) it is easier to control the impact angle and produce arrays of parallel tracks or create some particular angular distributions for getting rid of merging pores.

Very recent advances showed that with ion beam it is possible to control the number and the geometrical distribution of the tracks. For this aim, the sample is covered by

a metallic mask with a hole of small diameter (0.1 mm) so that the ions can penetrate the film only through the hole. By registering the ions passing through the film and shutting down and/or moving the membrane after one single ion had passed through [49, 50], it is possible to obtain single pore membranes or membranes with geometrically patterned arrays of tracks (and pores).

The limitations of the ion beam accelerator method are (a) the relative instability of the particle flux and (b) higher cost than irradiation.

In the past decade a decrease in the popularity of reactor-based irradiation facilities and an increase in the use of accelerators has been observed.

Chemical etching is the process of pore formation during which the damaged zone of a latent track is removed and transformed into a hollow channel (pore). The most widely used etching agents are alkali solutions (KOH or NaOH). During chemical etching, the damaged zone of a latent track is removed and transformed into a hollow channel [32]. The simplest description of the etching process is based on two parameters: the bulk etch rate (V_B) and the track etch rate (V_T). While V_B depends on the material, etchant composition, and temperature, V_T depends on additional parameters, such as sensitivity of the material, irradiation and postirradiation conditions, and etching conditions [32].

It was shown that a strict control of the etching conditions (material, etchant composition, and temperature) allows one to control the shape of the pores, obtaining, for instance, funnellike or conically shaped pores [35, 50]. In these cases etching is performed asymmetrically, so that $V_B > V_T$, this ratio changing through the thickness of the membrane. Typically, in a U-tube cell, the membrane separates an alkaline etching solution (usually KOH) from a stopping solution, typically a weak acid solution (HCOOH). A potential of some tens of volts is applied across the membrane by two Pt electrodes. The electrode in the etching solution serves as the anode, and the electrode in the stop solution is the cathode. The application of a potential across the membrane is stopped as soon as a monitoring ammeter registers an increase of current up to a preset value, typically 1 mA. The membrane is then immediately immersed (both sides) in the stopping medium, blocking the asymmetrical etching; at the end of the process, conical nanopores of controlled shape are obtained [25, 35].

3. MEMBRANE TEMPLATED DEPOSITION OF METALS

3.1. Electrochemical Deposition of Metals

Electrochemical deposition of metals in the pores of templating membranes requires that one side of the membrane be in direct contact with a metallic layer. This can be produced by plasma or vacuum deposition of a metal layer on one side of the membrane [51] or by tightly attaching the membrane on the surface of a solid electrode [5]. These procedures require that the membrane film be robust enough to tolerate this kind of manipulation; for plasma or vacuum deposition, the thickness required is usually >10 μm for track etched membrane and >30 μm for alumina membranes [51]. The metal which produces the conductive layer can be the same or different from the one that will provide the final template structure; in some cases, to improve adhesion of the sputtered or evaporated metal layer, a thin film of reactive metals such as chromium or titanium is deposited at first [52].

The scheme for electrochemical template synthesis is shown in Figure 2. For performing the template deposition, the coated film is placed in an electrochemical cell where the template membrane acts as the cathode and a counter electrode is the anode. The deposition can be carried out under galvanostatic or potentiostatic conditions.

The typical final products of the electrochemical deposition are solid nanoparticles and not hollow structures (such as nanotubes or nanocapsules). The electrochemical process consists in fact of the progressive growth and filling of the pores, starting from the bottom metallic layer and progressing toward the open end of the templating pore (see Fig. 2).

In a potentiostatic electrochemical deposition, three distinct regions characterize the time evolution of the current during the process. [53] With reference to the typical behavior shown in Figure 3, in region I metal wires grow in the pores, in region II the pores are completely filled, and in region III the growth proceeds on the outer face of the templating membrane. Stopping the electrodeposition at step I brings to the formation of nanofibers and at step II to "mushroom" shaped nanostructures [52].

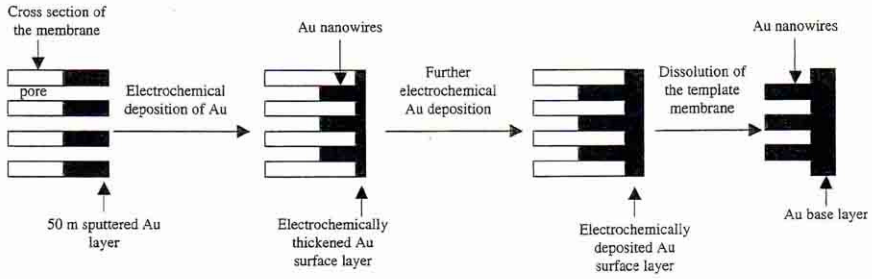

Figure 2. Scheme for electrochemical template synthesis.

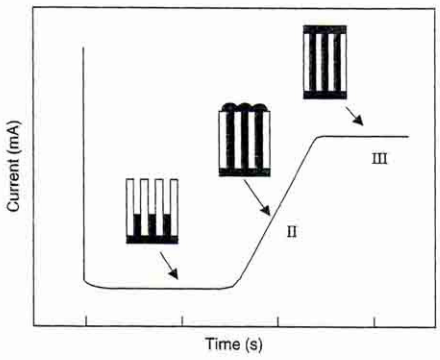

Figure 3. Dependence of the electrochemical reduction current on time for the potentiostatic deposition of a metal in a nanoporous membrane. In region I metal wires grow in the pores, in region II the pores are just completely filled (transition region to bulk growth), and in region III, growth commences over the whole membrane. Redrawn with permission from [53], T. M. Whitney et al., *Science* 261, 1316 (1993). © 1993, AAAS.

Electrodeposition of metals has been studied for obtaining gold nanowires in alumina [54–56], mica [23], and polycarbonate [52] microporous templates. Also other metals were studied with this respect, such as Co [52, 57–59], Ni [52, 58, 60], Cu [52, 61], Pt, and Pd [62]. With the goal of obtaining nanowires with special properties, even alloys such as NiFe [58], FeSiB [60], or salts such as Bi_2Te_3 [63, 64] and CdS [65] have been deposited electrochemically in nanoporous templates.

One problem encountered in electrochemical deposition of metals in polycarbonate template is related to the low wettability of this polymer, even after impregnation with polyvinyl pyrrolidone. To overcome this problem, Mallouk and co-workers proposed the addition of 1–2% gelatin to the electrodeposition baths [66–69].

3.2. Electroless Deposition of Metals

By taking into account that templating membranes are made of insulating material, the possibility to exploit chemical deposition methods such as electroless deposition should be considered.

Electroless metal deposition involves the use of chemical reducing agents to plate a metal from a solution onto a surface. The key requirement for this process is to arrange the chemistry so that the kinetics of homogeneous electron transfer from the reducing agent to the metal ion be very slow. A catalyst that accelerates the rate of metal ion reduction is then applied to the surface to be coated. As a consequence the metal ion is reduced preferentially at the surface, incorporating the catalyst so that only this surface is coated with the desired metal. The thickness of the metal film deposited can be controlled by varying the plating time [9].

The principles of electroless deposition in templates are exemplified for the typical case of Au deposition, as developed in Chuck Martin's laboratory for the template fabrication of nanoelectrode ensembles, nanotubes and other differently shaped gold nanomaterials. The electroless plating of gold [12] consists of three steps; at first a "sensitizer" (Sn^{2+}) is applied to surfaces (pore walls plus faces) of the template membrane. This is accomplished by simply immersing the membrane into a solution containing $SnCl_2$. The sensitized membrane is then activated by immersion into an aqueous silver ammonia solution, which causes a redox reaction in which the surface-bound Sn(II) is oxidized to Sn(IV) and Ag^+ is reduced to elemental Ag. As a result, the pore walls and membrane faces become coated with discrete Ag nanoparticles. The Ag-coated membrane is then immersed into an Au plating bath. The Ag particles are galvanically displaced by Au and the pore walls and membrane faces become coated with Au particles. These particles catalyze the reduction of Au(I) on the membrane surfaces using formaldehyde as the reducing agent. If the plating procedure is stopped after a relatively short time before the Au nanowires are obtained, Au nanotubes with the length of the complete thickness of the template membrane are formed within the pores. For filling completely the pores to obtain nanowires, the electroless plating must be elongated up to 24 h. In order to slow down the kinetics of the deposition the process is performed operating in vicinity of 0°C. The Au electroless plating bath can be composed by a commercial solution containing $NaAu(SO_3)_2$ (Oromerse Part B, from Technics Inc.) [12], but also homemade electroless plating bath have been used [70].

At variance with the electrochemical template deposition, in the electroless method the growth of the metal layer starts from the sensitised/activated sites located on the pore walls, so that the deposition progress from the pore walls to the center. This is the reason why by stopping the deposition at short time, hollow metal nanomaterials (e.g., nanotubes) can be prepared [71]. For the nanotube formation, the control of the electroless bath at pH $\approx$ 8 was proposed [72]. These nanotubes can be separated from the template membrane or can be kept in the template membrane. The last procedure allows one to obtain separation membranes with metalized pores [73, 74], whose inner surface can be functionalized chemically, by resorting, for instance, to well known thiols chemistry [72].

For the preparation of the so-called nanoelectrode ensembles, metal nanowires must be obtained and kept inside the guest membrane through a solid sealing with the polymer membrane. This is obtained by causing the shrinking of the polymer by heating the ensemble just above the glass transition temperature of the polymer (150°C for polycarbonate), after the deposition.

For some specific applications, mixed electroless/electrochemical deposition of metals inside the pores of template membranes has been used. As an example, the fabrication of Au–Te nanocable, with a radial metal–semiconductor structure was carried out by electrochemical deposition of Te inside Au nanotubes previously obtained by electroless deposition [75].

Also other metals such as Cu [76], Pd [77], and Ni–P [78] can be deposited in polycarbonate templates by suitable electroless deposition procedures.

3.3. Template Deposition of Conducting Polymers and Composites with Biomacromolecules

Electrically conducting polymers have been extensively studied owing to their great potential application in many fields [79, 80]. Many of these applications require the production of well-defined nanostructures and thus the synthesis of nanoscale conducting polymers, such as nanotubes, nanowires, and nanofibers, has attracted considerable attention [81, 82]. Among the different strategies reported in the literature to synthesize nanostructured polymers, such as the lyotropic liquid crystalline phase "soft" template [83], or the use of surfactants adsorbed onto flat surfaces to control the morphology during the synthesis [84], the structurally well-defined "hard" templates process represents an elegant approach [85]. It has been observed that the electronic properties of conjugated polymers in the nanophase are very different from those of their corresponding bulk materials. In fact, it has been shown that the preparation of a conductive polymer within the pores of microfiltration membranes can give the polymer a unique morphology and can also change the properties of the polymer, resulting in a dramatic increase in conductivity [86]. This aspect has been confirmed by X-ray diffraction and polarized infrared absorption spectroscopy measurements, which reveal a preferential growth of the polymer chains in the template-synthesized fibrils according to the axes of the supporting membrane [87]. In the oriented structure, the polymer chains can align more tightly, which can explain the observed conductivity enhancements and the greater tensile strength. Similar behaviors have been found for different conducting polymers such as polypyrrole (Ppy), polyacetylene (PAni), and poly(3-methylthiophene) (P3MeT) [86, 88]. The template synthesis concept can be extended to the realization of new nanostructured materials, including polymeric transition metal complexes with Schiff-base ligands [89] or other nonconventional conducting polymers (e.g., 1,2-diaminobenzene), which can be successfully used for biosensors design [90]. Mallouk and co-workers prepared gold-capped protein-modified polypyrrole nanowires by electrochemical growth in porous aluminium oxide as template; by this way nanowires of controlled length that can incorporate proteins for use in nanowire-based biosensors or in nanoparticle assembly through biomolecular interactions were obtained [91]. Moreover, composite nanowires based on polypyrrole and carbon nanotube (Ppy/CNT) have been prepared by a template-directed electrochemical synthetic route, involving the electropolymerization of Ppy into the pores of a host membrane in the presence of shortened and carboxylated CNT dopants [92]. By combining the attractive properties of CNTs and the nanostructured conducting polymers, new nanocomposite can be obtained, opening up new opportunities ranging from chemical sensors to molecular electronic devices.

Different authors suggest that, according to the nature of the compounds used for preparing nanomaterials (conducting polymers, metals, semiconductors) and the nature and structure of the membrane used as supporting substrate (pore wall chemistry, pore distribution), the resulting nanostructured compounds may be solid (nanofibrils) or hollow (nanotubules). For instance, Demoustier-Champagne [93] reported the preparation of smooth and uniform polypyrrole nanocylinders by using a homemade polycarbonate track-etched membrane with different pore sized distribution. On the other hand, Martin et al. showed that polyaniline grown in template does not form closed-up fibrils even after long polymerization times [85]. The reason that the polymer preferentially nucleates and grows on the pore walls is straightforward: the polycationic forms of these polymers are completely insoluble and may interact with the pore wall. Moreover, there is also an electrostatic component because the polymers are cationic and there are anionic sites on the pore walls.

Large interest has been recently devoted to the preparation of biocompatible polymer coatings, to be used as Substrate for cell growth and differentiation. Since these scaffolds are often used in long-term implantations, highly stable materials are desired that can endure the implantation process as well as the potential attack from biochemical agents that exist in biological tissue. Conducting polymers have been developed over the past decade for biomedical applications [94, 95]. One of the big advantages of the electrochemical polymerization of conducting polymers is that a number of different polyelectrolytes can be used as macromolecular counterions. For instance, conducting polymers offer a new and attractive route for localizing oligonucleotides and chromosomal DNA onto conducting surfaces [96]. Such incorporation has attracted considerable interest as a tool for tailoring the chemical and physical properties of the resulting polymer–polyelectrolyte composites and imparting appropriate activity, opening up new opportunities, including genoelectronic devices, genetic analysis, or probing of DNA charge transfer. Bioactive molecules, that can be grafted on polymer chains, are expected to influence the response of living tissues to which they would come in contact. In addition, a composite substrate that combines biological activity with electrical properties represents an excellent substrate for the growth of cells. The effective surface area of a bioactive support is critical in determining its electrical properties, in promoting interactions with cells and in providing a gradient in mechanical behavior. In order to improve the interface of scaffold and tissue, nanostructured biocompatible substrates must be developed. With the aim to improve the morphological and electrochemical properties of the composites, nanofibers of Ppy have been successfully obtained by the electrochemical polymerization of pyrrole inside the pores of an alumina-based membrane in the presence of large biomolecules, based on the glycosaminoglycans family, namely, hyaluronic acid (HA), heparin (Hep), and chondroitin (Chon) (see Fig. 4), in view of the consideration that the cellular responses to materials depend on structural properties on a nanometer scale. These biomolecules are naturally occurring polysaccharides, which can be ubiquitously found in the extracellular matrix of the body and have potential applications in tissue regeneration and angiogenesis. The electrochemical entrapment of biomolecules in PPy nanostructures involves the application of an appropriate potential to the template working electrode immersed in an aqueous solution containing both biomolecules and monomer [97]. A scanning electron micrograph of a PPy-Hep electrode, after the dissolution of

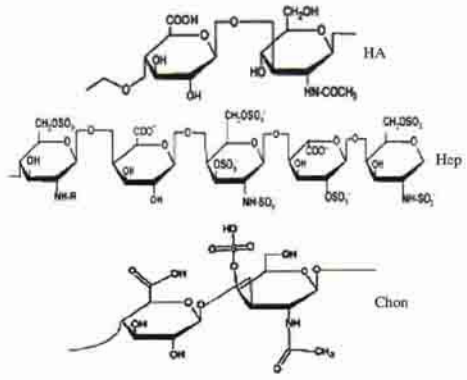

Figure 4. Structures of hyaluronic acid (HA), heparin (Hep), and chondroitin A sulfate (Chon).

the supporting porous alumina membrane, is reported in Figure 5. The image clearly shows that PPy-Hep samples form hollow oriented nanotubes. The nature and the distribution of the external charges play an important role in the physicochemical properties of the nanostructured PPy electrodes. The redox process, for example, which involves a cation doping and solvent motion according to the reaction

$$x(\mathrm{Ppy})^{z+}\mathrm{Hep}^{z-} + z\mathrm{K}^{+} + ze^{-} \Leftrightarrow x(\mathrm{Ppy})\mathrm{Hep}^{z-}z\mathrm{K}^{+}$$

does not show any kinetics limitation even at high scan rate (up to 200 mV/s) but assures high reversibility and elevated quantity of exchanged charge. Figure 6 compares the voltammetric scan of PPy-Hep in the form of both nanotube

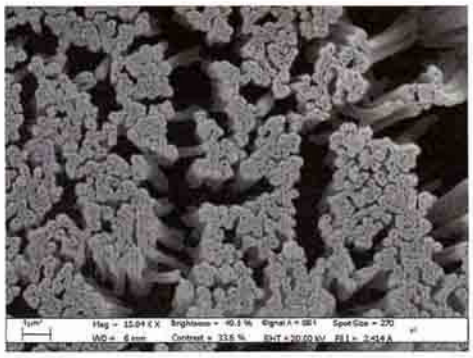

Figure 5. Scanning electron micrograph of a PPy-Hep composite electrode, after the dissolution of the Al_2O_3 templating membrane (membrane thickness 60 μm and pore diameter 100 nm). Synthesis conditions: potentiostatic synthesis at 0.8 V versus SCE (charge = 0.2 C/cm^2) using an aqueous solution of Py (1 M) and Hep (5 mg/ml). Pt counter electrode, room temperature.

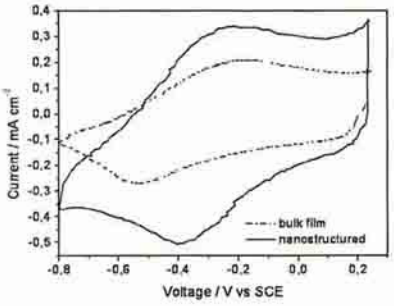

Figure 6. Comparative cyclic voltammetry of PPy-Hep electrodes (as film or nanoelectrode) in 1 M KCl supporting electrolyte. Scan rate 20 mV s^{-1}. Pt counter electrode.

and bulk sample; it confirms that the nanostructured electrode shows better electrochemical characteristics than the bulk film.

It is important to note that, by using a proper synthetic route, it is possible to create a favorable biocompatible surface able to promote interfacial interactions between proteins and the electronic surface. In this respect, the nanostructured polymeric materials offer many advantages over other strategies aimed to modify bioelectronic interfaces. First they provide a proper molecular architecture that can be controlled during the deposition process by choosing both the applied potential and the nature of the counterion. Moreover, the electrodeposited polymers can be use to functionalize a wider range of different active surfaces, including carbon or composite substrates. Consequently, it is possible to change the conductivity, the thickness, and the porosity of the interfaces and ultimately, in the future, to make implantable three-dimensional electrode with higher surface areas, able to promote biomolecular interactions.

In this respect, from nanotechnology it is only one step to nanomedicine, which may be defined as the monitoring, repair, construction, and control of human biological systems at the molecular level, using engineered nanodevices and nanostructures. Nanomedicine is both a destination and a journey. The journey will cross new frontiers, uncover new knowledge, and bring new horizons to the understanding and practice of medicine.

4. TEMPLATE NANOELECTRODE ENSEMBLES

Nanoelectrode ensembles and arrays (NEA) are advanced nanostructured electrode systems that are finding application in a variety of fields ranging from sensors to electronics, from energy storage to magnetic materials [9]. The difference between NEEs and NEAs is that in the former the spatial distribution of the nanoelectrodes is random, while in the array it is ordered. In the following we will refer mainly to NEEs prepared using microporous membranes as templating systems and containing random distributed pores.

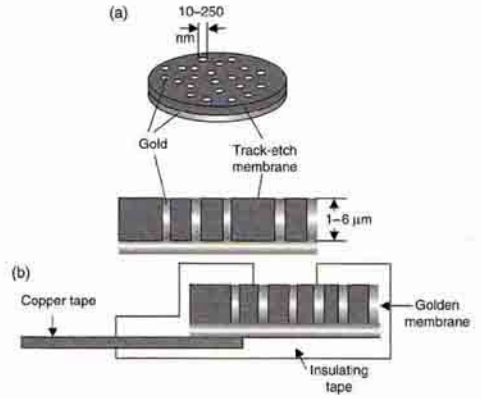

Figure 7. (a) Scheme of a Au NEE deposited at a polycarbonate membrane. (b) Schematic diagram of the typical assembly of the nanoelectrode ensembles.

They are prepared by filling with metal nanowires the pores of a template so that in the final ensemble, only the surface of the nanodisc is exposed to the sample solution. The density of the pores in the template determines the number of Au-disk nanoelectrode elements per centimeter squared of NEE surface and, correspondingly, the average distance between the nanoelectrode elements. The scheme of a NEE together with the typical assembly used to transform a piece of golden membrane into a handy NEE are shown in Figure 7. Specific details can be found in the first original papers [12, 98], as well as in recent reviews [8, 9, 99]. At the present status of research, in this kind of NEEs all the nanoelectrodes are connected to each other by a back metal current collector, so that all the nanoelectrodes experience the same applied potential.

Concerning the kind of membranes used as template it can be noted that track-etched polymer membranes are preferred for NEEs preparation with respect to alumina ones, since track-etched membranes are characterized by smaller pore densities. From an electroanalytical viewpoint this is an important feature, since it reduces the reciprocal interactions between the individuals nanoelectrode elements (see below).

As illustrated in Figure 8, depending on whether the template is kept on site, partially etched or fully removed, it is possible to obtain nanoelectrodes ensembles with very different geometries. Theoretical treatment of the electrochemical behavior of these different geometries is still at a preliminary stage. Such analysis was developed systematically only for the nanodisk case, as will be presented in the following section.

4.1. Diffusion at Ensembles of Nanodisk Electrodes

The electrochemical characteristics that distinguish nanodisk electrode ensembles (NDEE) from conventional macro (mm-sized) or even ultramicro (μm-sized) electrodes are dramatic lowering of double-layer charging (capacitive) currents [2, 12] and extreme sensitivity to the kinetics of the charge transfer process [100], which means capability to measure very high charge transfer rate constants [13].

Since these characteristics are peculiar to ensembles of nanodisks electrodes, in case of experimental inability to get direct morphological information on the NDEE structure by, e.g., electron or scanning probe microscopy [101], the lack of some of these characteristics, such as the persistence

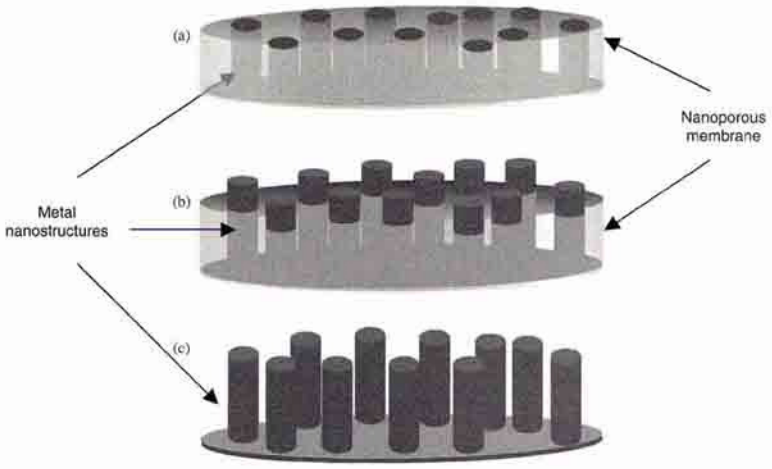

Figure 8. Different geometries for templated nanoelectrode ensembles: (a) ensemble of nanodiscs; (b) ensemble of partially naked nanowires; (c) ensemble of completely naked nanowires.

of high capacitive currents, should be taken as a diagnostic indication of a failure in the preparation procedure.

From a voltammetric viewpoint, NDEE can be considered as ensembles of disc ultramicroelectrodes separated by an electrical insulator interposed between them. An ultramicroelectrode is considered as an electrode with at least one dimension comparable to or lower than the thickness of the diffusion layer (typically <25 μm). At such small electrodes, edge effects from the electrode become relevant and diffusion from the bulk solution to the electrode surface is described in terms of radial geometry instead of the simpler linear geometry used for larger (>100 μm) electrodes. A NDEE can be considered as a very large assembly of very small ultramicrolectrodes confined in a rather small space. Since the number of nanodiscs elements/surface is large (10^6–10^8 elements/cm^2), all the nanoelectrodes are statistically equivalent and the different contribution of the elements at the outer range of the ensemble can be considered negligible [102, 103] even in NDEEs of overall area as small as 10^{-2}–10^{-3} cm^2 [102].

NDEEs can exhibit three distinct voltammetric response regimes depending on the scan rate or reciprocal distance between the nanoelectrode elements [104, 105]. When radial diffusion boundary layers overlap totally (radius of diffusion hemisphere larger then average hemidistance between electrodes, slow scan rates) NDEEs behave as planar macroelectrodes with respect to Faradaic currents (total overlap conditions). When diffusion hemispheres become shorter (higher scan rates), the current response is dominated by radial diffusion at each single element (pure radial conditions). At even higher scan rates, the linear active state is reached in which the current response is governed by linear diffusion to the individual nanodisc (linear active conditions). Figure 9 sketches the situation encountered for the total overlap and pure radial regimes. Being characterized by the higher signal/background current ratios (see below), these two regimes are those typically used for analytical and sensing applications.

The diffusion regime usually observed at NDEEs prepared form commercial track-etched membranes is the total overlap regime [12]. Transition from one regime to the other as a function of nanoelement distance was demonstrated experimentally [104] using specially made membranes.

4.2. Signal to Background Current Ratios

Under total overlap diffusion regime, NDEEs show enhanced electroanalytical detection limits, relative to a conventional millimeter-sized electrode. This is because the Faradaic current (I_F) at the NDEE is proportional to the

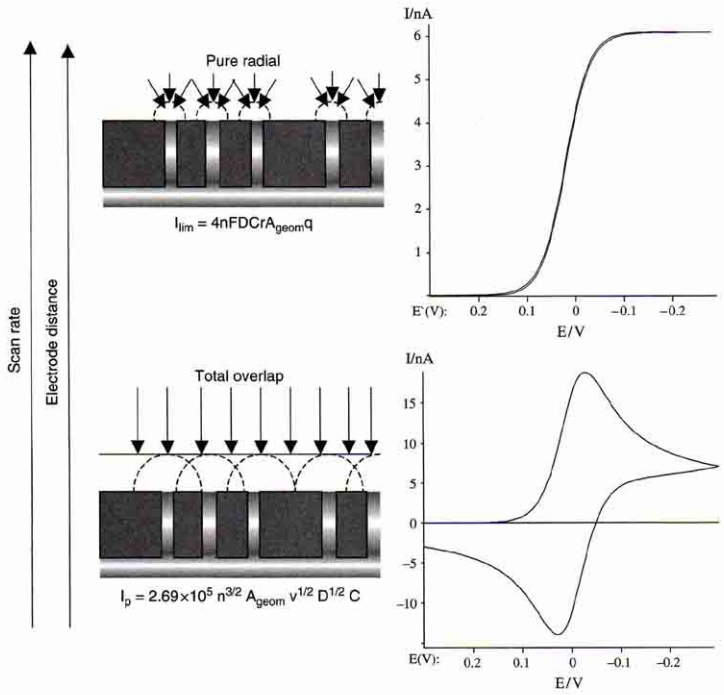

Figure 9. Typical diffusive regimes observed at nanoelectrode ensembles as a function of the scan rate and/or nanoelectrodes distance.

total geometric area (A_{geom}, nanodiscs plus insulator area) of the ensemble, while the double-layer charging current (I_C) is proportional only to the area of the electrode elements (active area, A_{act}) [12]; in voltammetry, I_C is the main component of the noise.

Faradaic-to-capacitive currents at NDEEs and conventional electrodes with the same geometric area are related by Eq. (1) [12, 99]:

$$(I_F/I_C)_{NDEE} = (I_F/I_C)_{conv} A_{geom}/A_{act} \quad (1)$$

This ratio at the NDEE is higher than the relevant ratio at a conventional electrode of the same geometric area for a proportionality factor that is the reciprocal of the fractional electrode area (f) defined as

$$f = A_{act}/A_{geom} \quad (2)$$

Typical f values for NDEEs are between 10^{-3} and 10^{-2}. As shown in Figure 10, faradaic currents at NDEEs are equal to those recorded at macro electrodes of the same geometric area, however, at NDEEs background currents are dramatically lowered. As a consequence, signals for analytes at concentrations lower than micromolar are significatively better resolved from the background current. Such an improvement in the Faradaic to capacitive currents ratio explains why detection limits (DLs) at NDEEs can be 2–3 orders of magnitude lower than with conventional electrodes [2, 12, 106].

The cyclic voltammograms in Figure 11 show that improvements in signal/background current ratios at NDEEs

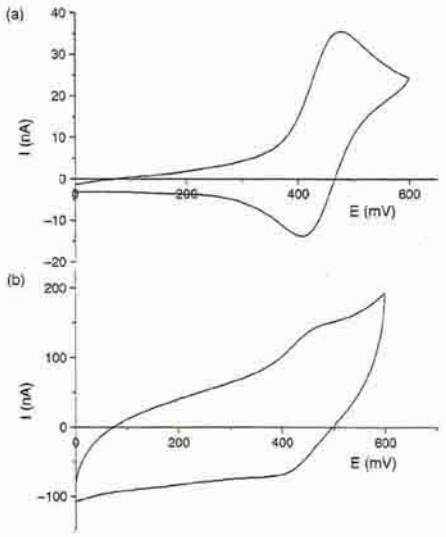

Figure 10. Cyclic voltammograms recorded at NEEs (a) in 5 μM FA^+ 10^{-3} M $NaNO_3$ solutions; scan rate 20 $mV s^{-1}$; A_{geom} = 0.07 cm^2, and (b) Au macroelectrode.

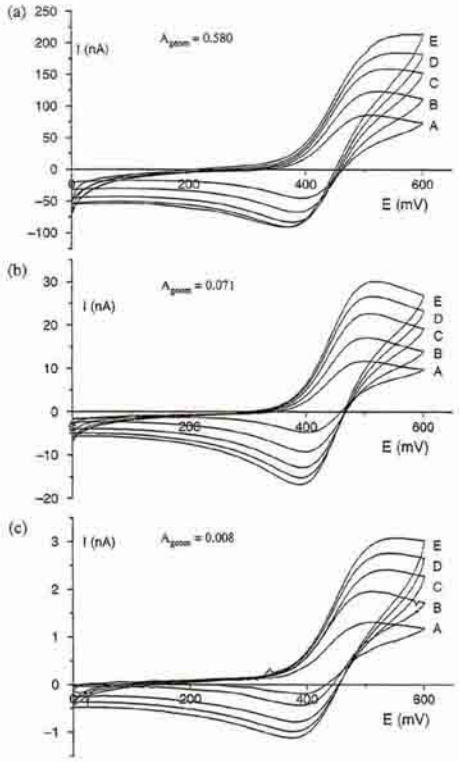

Figure 11. Cyclic voltammograms recorded at NDEEs with different geometric areas: (a) 0.586 cm^2, (b) 0.071 cm^2, and (c) 0.008 cm^2, in 5 μM FA^+ 10^{-3} M $NaNO_3$ solution, at different scan rates of (A) 2 $mV s^{-1}$; (B) 5 $mV s^{-1}$; (C) 10 $mV s^{-1}$; (D) 15 $mV s^{-1}$; and (E) 20 $mV s^{-1}$. Reprinted with permission from [102], L. M. Moretto et al., *Talanta* 62, 1055 (2004). © 2004, Elsevier.

are independent of the total geometric area of the ensemble [102]; this is true if the fractional area is kept constant and if the dimensions of the ensemble are lowered to a size still large enough to contain a large number of nanoelements (for instance, NDEE with A_{geom} of 0.005 cm^2 contains 4.8×10^6 nanoelectrodes). Note that NDEEs warranty such independence on the ensemble size for overall geometric areas much lower than those required for achieving comparable results with arrays of micrometer sized electrodes [103]. This is particularly attractive when thinking of applying the advantages of the use of arrays/ensembles of micro-nanoelectrodes to analyses in samples of very small volume or for "*in vivo*" biomedical applications.

For a given overall geometric area, it is evident that the I_F/I_C is maximum when the total overlap regime is operative, being lower in the case of a pure radial regime. In this case, in fact, only a certain percentage of the geometric area

of the ensemble contributes to producing a Faradaic current, while in the total overlap regime, this percentage is 100%. On the other hand, it is worth stressing that for NDEEs or NEAs with the same active area, higher Faradaic currents are achieved when operating under pure radial conditions [103]; this is the regime of choice for obtaining the maximum improvement of detection limits when there is no constrain in increasing the distance between the nanoelectrode elements and/or the overall geometric area of the ensemble.

When using Au-NDEEs for trace analysis the accessible potential window results influenced by the effect of the high amplification levels on the background signals. The accessible limit depends indeed on the current scale (e.g., nA or pA) at which the signal is recorded and is really an arbitrary definition. Working at nA scales, on the positive side the accessible limit is about 0.7 V versus Ag/AgCl and is related to the formation of a surface oxide layer [12]. On the negative side it depends on the hydrogen evolution reaction and shifts negatively by increasing the solution pH (e.g., approximately −0.75 V vs. Ag/AgCl at pH 7) [106].

It was shown that NDEEs can be advantageously used note only as naked nanoelectrode ensembles but also as polymer coated devices [2]. For instance, the overall surface of a NDEE (insulator and nanodiscs) can be easily coated by a thin layer of an ionomer coating. In the cited literature example [2], the ionomer of choice was the poly(ester sulfonate) Eastman AQ55®, which was applied as a water dispersion, i.e., using a solvent which does not damage the NDEE surface (the polycarbonate template can be damaged by organic solvents). Really, such an approach showed that it was possible in this way to combine successfully the preconcentration capabilities of ionomer coated electrodes [8, 98, 107] with the increased Faradaic/capacitive current ratio typical of NDEEs.

The ability of NDEEs to furnish well-resolved cyclic voltammograms for trace redox species has interesting consequences also for adsorption related problems, as in the case of small organic redox molecules and some biomacromolecules as well. If adsorption is concentration dependent, then lowering the solution concentration below the adsorption limit can sometimes overcome the problem. This was demonstrated to be the case for some phenothiazines [106], commonly used as redox mediators in biosensors, and for the heme-containing enzyme cytochrome *c* [108].

4.3. Electron Transfer Kinetics

An important characteristic of NDEEs is that electron transfer kinetics appear slower than at single electrodes [12]. Being composed of a large number of nanodiscs, metal elements surrounded by a large surface of insulating material (the guest membrane), NDEEs can be considered as electrodes with partially blocked surfaces (PBE); the nanodisc electrodes are the unblocked surfaces and the template membrane is the blocking material. According to the pioneering model elaborated by Amatore et al. [100], the current response at this kind of electrodes is identical to that of a naked electrode of the same overall geometric area, but with a smaller apparent standard rate constant for the electron transfer, which decreases as the coverage with the blocking agent increases. Such an apparent rate constant (k°_{app}) is related, in fact, to the true standard charge transfer rate constant (k°), by the relationship [100]

$$k^{\circ}_{app} = k^{\circ}(1 - \vartheta) = k^{\circ} f \tag{3}$$

where ϑ is the fraction of blocked electrode surface and f is the fraction of the electrode surface that is Au nanodisc (see Eq. (2)).

Table 3. Examples of analytical applications of nanoelectrode ensembles.

Analyte	Comments	Ref.
Ferrocene derivatives, $Ru(NH_3)_6^{3+}$	Fundamentals for the fabrication and characterization of Au-NDEEs are given. It is shown that DL can be 3 orders of magnitude lower than with regular electrodes.	[12]
Ferrocene derivatives, $Ru(NH_3)_6^{3+}$	NDEEs coated with polyester sulfonate are used for preconcentration and trace analyses of redox cations. DLs are in the 10^{-9} M range.	[2]
$Fe(CN)_6^{4-}$	NDEE fabricated by self-assembly of Au colloidal nanoparticles. Electrode density depends on self-assembly time. DL = 1×10^{-6} M.	[112]
Phenotiazine, methylviologen	Cathodic limit at Au-NDEE is examined. Detection limits depend on reduction potential: DL = 1.2×10^{-7} M for phenothiazine, 2×10^{-6} M for methylviologen.	[106]
Cytochrome *c*	Au-NDEE detects the direct electrochemistry of cyt *c* even in the absence of promoters. Dilute solutions avoid adsorption problems. DL = 1×10^{-5} M by CV and 3×10^{-8} M by DPV.	[102, 108]
NO	Pt-NDEE in an alumina template is designed for NO determination *in vitro* and *in vivo*. Interfering anions are rejected by a Nafion® coating. DL = 1×10^{-8} M.	[113]
Glucose	Au nanotubular electrode ensemble used for in flow detection of glucose. Glucose oxidase immobilized via bonding to self-assembled monolayers deposited on Au. DL = 2×10^{-4} M.	[114]
Glucose	Carbon nanotube (CNT)-NEE is fabricated. Glucose oxidase immobilized on CNT via carbodiimide. H_2O_2 detected catalitically by CNT. DL = 8×10^{-5} M.	[115]
DNA duplex	Interdigited array of 100-nm electrodes fabricated by e-beam lithography. DNA attached to Au and 10^{-4} M Ru $(NH_3)_6^{2+}$ used as redox intercalator. Characterization of *ss*- and *ds*-DNA of 15 nucleotides performed.	[116]
DNA duplex	NEA of multiwalled CNT embedded in SiO_2. DNA attached to CNT via carbodiimide. Detection by $Ru(bpy)_3^{2+}$ mediated guanine oxidation.	[117]
DNA duplex	3-D NEEs (nanowires) are obtained by partial etching with oxygen plasma from NDEEs in polycarbonate template. Detection of duplex formation at atomole-level is achieved by Ru(III)/Fe(III) electrocatalysis.	[118]

Such dependence has two different practical consequences. From a mechanistic viewpoint, it is an advantage since it means that with NDEEs it is easier to obtain experimentally very large k° values [109]. What is measured at NEE is the smaller k°_{app}, which can be converted into the larger k° by Eq. (3) [13, 106].

Further understanding of the electrochemical behavior of NDEEs will probably take advantage from recent studies devoted to modeling by digital simulation the voltammetric behavior of regular [110] and random arrays [111] of ultramicroelectrodes.

4.4. Analytical and Sensing Applications

The ability of NEE to furnish well-resolved cyclic voltammograms allowed researchers to develop sensitive methods for trace determinations of redox species characterized by fast electron transfer kinetics. For this reason, the analytes of choice for such applications are mainly redox molecules displaying very reversible voltammetric behavior as those typically employed as electron transfer mediators in biosensors. Note that lowering the background noise (related to the capacitive current) in an electrochemical determination improves not only the detection limit but also the precision of the determination.

Table 3 lists some analytical application of NEE, which up to now are oriented mainly to the electrochemical biosensor field. It is worth noting that the application of NEE for analytical purposes is just beginning and is expected to grow quickly and the number of real examples will quickly widen.

5. NANOELECTRODES ENSEMBLES FOR BATTERIES

The widespread market of consumer electronics with the related and constantly growing commercialization of popular portable devices, such as cellular phones, PDAs, and notebooks, relies on the availability of efficient and sustainable powering systems, namely, of high-energy, low-cost, and environmentally compatible, rechargeable batteries [119]. At beginning of this market, say in the early 1980s, portable consumer electronics had the constraint of the use of at-that-time available batteries, such as the lead-acid or nickel-cadmium batteries. It was immediately clear that these first generation batteries were inadequate for the purpose, mainly because of their low energy density, i.e., limited to 40–60 W h/kg.

Indeed, the first portable devices were heavy and bulky and had very limited operational time, this being mainly associated to the high weight and large volume of their power sources. In addition, both lead-acid and nickel-cadmium batteries contain materials with a degree of toxicity which may induce severe environmental risk. Thus, alternative systems, capable to assure long life associated with low weight and low volume, were highly requested and the battery technology adapted by developing a second-generation battery system, i.e., the nickel-metal hydride battery. Effectively, this battery, with its energy density content of the order of 60–70 W h/kg, allowed one step forward in terms of dimension and weight of the portable devices. However, the real breakthrough in this field was achieved with the advent of the lithium ion battery. This battery, with its 150 W h/kg value of energy density, is now the power source of choice for portable devices, today a multimillion dollar market.

However, the consumer electronics market is in continuous evolution with the production of diversified multifeature devices, which require constantly increasing power levels. Therefore, it is expected that even the lithium ion battery will soon become inadequate to meet increasing user demands. In addition to the consumer electronics area, high-energy batteries are also urgently requested for facing the great challenge of the new millennium, namely, a change of the energy policy and a more accurate control of the environment of the planet. In response to these needs, which, among others, call for a wider use of clean energy sources and of controlled- or zero-emission vehicles in large urban areas, it is now essential that high-energy, low-cost, and environmentally friendly storage systems are identified. Lithium batteries can be good candidates for all these application, provide that their performances reach a level higher than that presently offered.

Generally, the performance of any device depends intimately on the properties of the materials on which they are formed; this holds also for lithium batteries. The chemistry of these batteries has not changed since their introduction in the market in the early 1990s. Basically, a lithium ion battery consists of a lithium ion intercalation negative electrode (generally graphite) and a lithium ion intercalation positive electrode (generally the lithium metal oxide $LiCoO_2$ or, occasionally, the lithium manganese spinel $LiMn_2O_4$), these being separated by a lithium ion conducting electrolyte, for example, a solution of $LiPF_6$ in an ethylene carbonate-diethylcarbonate, EC-DEC, mixture [120, 121].

As already pointed out, although lithium ion batteries are still a commercial success, it is also clear that they are reaching the limits in performance by using the current electrode materials [122]. For the new generations of rechargeable lithium batteries, not only for application in consumer electronics but especially for clean energy storage and powering electric or hybrid vehicles, a further step in performance, this in turn being related to a breakthrough in materials, is essential. Nanotechnology is the best tool for achieving this breakthrough, since it provides the conditions for greatly improving the performance of the battery electrode materials. It is in fact expected that passing from bulk to nanostructures, one may,

(i) favor higher interfacial area, this leading to higher charge/discharge rates,
(ii) provide short path lengths for Li^+ ion transport, this resulting in increase in power capabilities,
(iii) achieve accommodation of the strain of lithium insertion/removal, this improving cycle life.

Indeed, these beneficial aspects are now confirmed and nanostructured materials are becoming increasingly important for electrochemical energy storage [10, 11] and for lithium batteries in particular [123, 124]. In this section we will attempt to review the progress in this area with the description of the results obtained at the anode, the cathode, and the electrolyte side of these new types of electrode nanostructures.

As already mentioned, graphite is the most common anode material used in the present lithium ion battery configuration. Graphite has a good cycling stability but a relatively low specific capacity, i.e., not exceeding 372 mA h/g. Thus, if an improvement in energy content is desired, new, high-capacity alternative anode materials have to be developed. In this respect, metals that store lithium are among the best candidates. Indeed, a number of metals and semiconductors, for example, Al, Sn, and Si, react with lithium to form alloys by electrochemical processes that involve a large number of atoms for formula units, thus providing a specific capacity much larger than that of conventional graphite [125–127]. For instance, the lithium-silicon alloy has, in its fully lithiated composition Li_4Si, a theoretical specific capacity of 4200 mA h/g, i.e., a value 1 order of magnitude larger than that of conventional graphite. Other examples are given in Table 4.

Unfortunately, the accommodation of this large amount of lithium is accompanied by enormous volume changes in the host material. These in turn induce severe mechanical strains, which lead the electrode to crack and, eventually, disintegrate after a few cycles. An illustrative example is provided in Figure 12, which shows the evolution of the morphology of an aluminium electrode in the course of the initial charge (lithium alloying)–discharge (lithium removal) cycles in a lithium cell.

A way to solve this problem is to modify the morphology of the metal alloy electrodes by reducing their particle size to a few nanometers and/or by designing special nanostructures. Indeed, this strategy is expected to have a twofold effect on the performance of the electrodes:

(i) improvement in cycling stability, since small particles more easily accommodate the mechanical strains (the absolute volume changes are smaller than for larger particles, although the relative changes are the same), and
(ii) enhancement of power due to the reduction of the lithium ion diffusion length. The validity of this strategy has been confirmed by various authors [128–130].

Undoubtedly, alloy performance can benefit from nanostructures. For instance, thin amorphous silicon films deposited on a specially roughened copper foil surface were shown to have close to 100% reversibility at capacities exceeding 3000 mA h/g [131]. Good capacity retention was also found for silicon electrodes prepared with a nanopillar surface morphology, see scanning electron microscope (SEM) image of Figure 13 [132]. In this case the stability of the electrode was obtained by size confinement, which alters particle deformation and reduces fracturing.

Table 4. Theoretical specific capacity for selected lithium storage metals in comparison with graphite and metallic lithium.

Unlithiated material	Fully lithiated material	Gravimetric capacity (mA h/g)	Volumetric capacity (mA h/cm^3)
Al	LiAl	993	1374
Sn	$Li_{4.4}Sn$	994	2025
Si	Li_4Si	4200	2323
C, graphite	LiC_6	372	760
Metallic lithium	Li	3860	2047

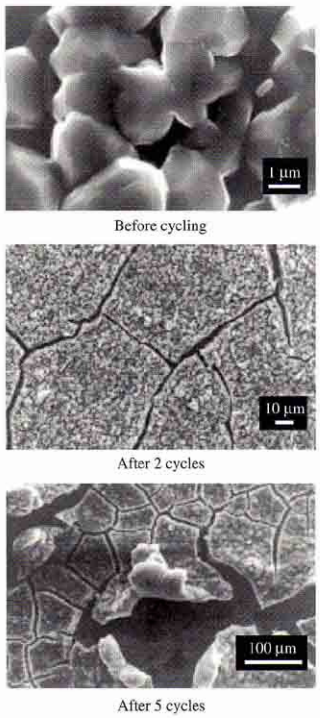

Figure 12. Changes in the morphology of a tin electrode after charge (lithium alloying)–discharge (lithium removal) cycles in a lithium cell. The mechanical strain generated during the cycles leads to cracking of the electrode with resulting marked loss of capacity in the course of a few cycles. Reprinted with permission from [126], M. Winter and J. O. Besenhard, *Electrochim. Acta* 45, 31 (1999). © 1999, Elsevier.

Another strategy for limiting the effect of the volume changes and thus to assure electrode integrity is based on the active/inactive nanocomposite concept. There are several papers describing this approach, which basically involves the intimate mixing of two materials, one reacting with lithium and the other acting as an inactive confining buffer to accommodate the volume changes and, thus, the associated electrode strain [128–130]. Indeed, by applying this concept through different systems, considerable improvement in the electrode cycle life has been reported.

Nanostructures are also highly beneficial for other classes of alternative electrode materials, e.g., for metal oxide electrodes. For instance, it is known that tin oxide can electrochemically react with lithium with a first process involving the formation of lithium oxide and tin, followed by a Li–Sn alloying–dealloying reversible process [133]. It is assumed that the "*in situ*" formed lithium oxide can act as a "buffer" for accommodating the volume changes that accompany the

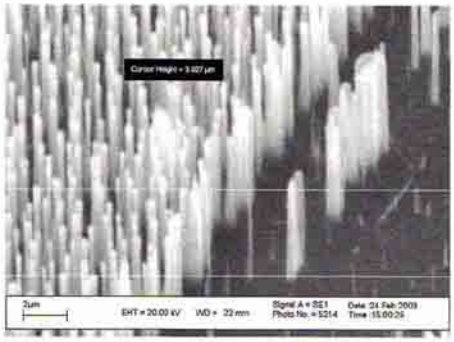

Figure 13. SEM image of a silicon electrode having a nanopillar surface morphology. This morphology provides free volume configurations, which are able to accommodate the massive volume changes occasioned by lithium alloying/dealloying. Courtesy of Prof. Mino Green from Imperial College, London.

second alloying process [134]. However, if common electrode morphologies are used, the cycling stability of the tin oxide electrode is still unsatisfactory [135].

Also, in this case, considerable improvements are obtained moving to nanostructures. Figure 14 shows the morphology of tin oxide prepared in the form of nanowires using a specific template technique [136]. This technique leads to electrode morphologies consisting in nanowires or nanotubes of Li^+ insertion materials that protrude from an underlying current collector surface like the bristles of a brush [27, 29, 85]. This template method is a general approach for preparing nanostructures containing the desired electrode material within the pores of an usual polycarbonate membrane with pore diameter of the order of 100 nm. The electrode material is deposited within the pores

Figure 14. SEM image of a tin oxide electrode having a nanofibril morphology. The structure consists of nanodisperse 110-nm SnO_2 fibers protruding from a current-collector surface like the bristles of a brush. Reprinted with permission from [136], Li et al., *J. Power Sources* 97, 240 (2001). © 2001, Elsevier.

of the membrane by a solution-based method. For instance, in the case of the SnO_2 preparation, the membrane was immersed in a solution of $SnCl_2$, HCl, and ethyl alcohol and then applied to the surface of a Pt current collector [136]. The membrane is then removed by burning it in oxygen plasma. This leaves nanofibers of the desired electrode materials, which in the case of SnO_2 were 110 nm in diameter and 6.0 μm in length, see the SEM image reported in Figure 14.

This procedure gives unique electrode structures having dramatically improved rate and cycling performance associated with the small size of the nanofibers and the small domain size of the metal alloy grain within the nanofibers. For instance, tests in a lithium cell have demonstrated that the nanofiber SnO_2 electrode is able to operate at rates as high as 8 C with a stable capacity of the order of 700 mA h/g [136], values never achieved with conventional electrode structures, such as graphite.

Nanomaterials consisting of nanoparticles or nanoarchitectured materials may also have some potential disadvantages associated to their high external surface area, which may lead to excessive side reactions with the electrolyte and hence capacity losses or poor calendar life. Such problems may be addressed with internally nanostructured materials where the particles are significantly larger than the nanodomains. This can have the advantage of reducing side reactions with the electrolyte, compared with those of nanoparticulate materials, and of ensuring higher volumetric energy densities [124]. An example of these internally nanostructured anodes includes a family of transition metal oxides such as CoO, CuO, NiO, Co_3O_4, and MnO [137]. The full electrochemical reduction of these oxides versus lithium involving two or more electrons per 3d metal leads to composite materials consisting of nanometer metallic clusters dispersed in an amorphous Li_2O matrix exhibiting high reversibility and providing large capacities that can be maintained for hundreds of cycles. Such results turn out not to be specific to oxides but can be extended to sulfides, nitrides, or fluorides or to other families of compounds (e.g., borates, vanadates) [138].

Also critical for the progress of lithium batteries are improvements at the cathode side. For instance the replacement of the high cost, partially toxic $LiCoO_2$ with more affordable and sustainable materials would be highly welcomed. The nanotechnology approach is here much less developed than in the case of the anodes. In fact, the use of nanoparticulate forms of the classical cathode materials such as $LiCoO_2$ can lead to significant reaction with the electrolyte and ultimately safety problems (one of the most critical issues for lithium batteries) especially at elevated temperatures, compared with the use of such materials in the micrometer range. Therefore, the nano approach may be safely adopted for those electrode materials having voltage profiles falling within the stability window of the electrolyte. In these cases, the many advantages of nanoparticles may more easily be exploited. An example is the phospho olivine $LiFePO_4$ that, in a lithium cell, may be reversibly delithiated to $FePO_4$ with an operating voltage averaging around 3.5 V versus Li, i.e., a value largely within the stability window of the most common lithium ion electrolytes. Indeed, $LiFePO_4$ is an appealing cathode for lithium batteries: it is cheap, environmentally benign, and has a reasonably high

capacity, i.e., approaching that of $LiCoO_2$ (170 mA h g^{-1} vs. 220 mA h g^{-1}) [139].

However, the kinetics of this electrode are controlled by its poor electronic conductivity and by the low lithium ion diffusion across the reaction phases. Morphological modification at the nanoscale level appears the proper tool to control these undesired phenomena. Recent literature has shown that strategies such as carbon nanopainting [140], nanofibril textures [141], and carbon nanodispersion [142] led to excellent improvements in the utilization of the "*per se*" insulating $LiFePO_4$.

It has also been demonstrated that dispersion in the course of the synthesis of metal (e.g., Cu or Ag) powders at the nanoparticle size produces $LiFePO_4$ electrodes with enhanced electrochemical properties [143]. It is believed that the nanopowders act as nucleation sites for the growth of the $LiFePO_4$ particles, as well as conducting bridges between them, this finally resulting in an improvement of the infra- and interconductivity of the particles. Indeed, tests in lithium cells have demonstrated that these metal composite $LiFePO_4$ electrodes can cycle with good capacity delivery at room temperature and at high rates [143].

Another strategy for enhancing the performance of $LiFePO_4$ electrodes is that of preparing them in a nanofibril structure following a procedure similar to that used for the preparation of nanostructured tin oxide electrodes, see above. A sol–gel method was used to deposit the $LiFePO_4$ nanofibers within the pores of the template membrane, see Figure 15(A). Contrary to the usual procedure where the template is totally removed to yield nanofibers protruding from an underlying current collector surface, in this case the polycarbonate membrane was pyrolyzed in a reducing environment in order to yield graphitic carbon particles intimately mixed with the $LiFePO_4$ nanofibers, to finally obtain a nanocomposite $LiFePO_4$/carbon matrix [144]. Figure 15(B) shows a SEM image which clearly shows the carbon film coating on the $LiFePO_4$ nanofibers [144].

This $LiFePO_4$/carbon nanocomposite electrode structure is suited for high rate applications because the distance that Li^+ must diffuse in the electrode is limited by the radius of the nanofibers and because the carbon matrix provides for good electronic contact through the composite. Indeed, electrochemical tests in lithium cells have confirmed that these nanocomposite electrodes can deliver a capacity of 150 mA h/g at a rate of 5 C and maintain a substantial fraction of the theoretical capacity even at rates exceeding 50 C [144].

Finally, it has to be pointed out that progress in lithium batteries relies on improvement in electrolytes as well as in electrodes. Good practical results are expected by combining the use of templated nanofibers electrodes with the use of nanostrucutured polymer electrolytes based on poly(ethylene oxide) (PEO), suitable lithium salts, and ceramic nanoparticles [145–153].

Clearly there are pros and cons in any new approach. However, the results quoted in this short review chapter show that moving from traditional bulk structures to nanostructures can significantly change the electrode and electrolyte properties and, consequently, their performance in electrochemical devices, this being particularly valid for the case of lithium batteries. Although some risk may be

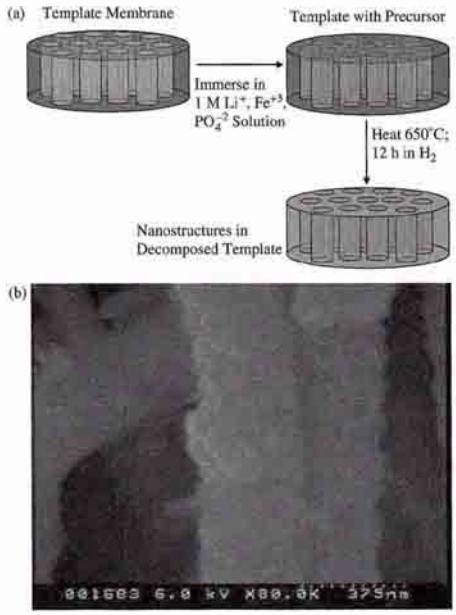

Figure 15. Scheme of the template synthesis of $LiFePO_4$/carbon electrode (a) and SEM image of a nanofiber of $LiFePO_4$ (b). The diameter of the fiber is around 200 nm.

associated with the high surface area of nanostructured electrode materials, nanotechnology is the right tool for yielding quantum jumps in battery performance. Indeed, by an appropriate selection of the battery materials, issues such as reactivity with the electrolyte and associated poor calendar life may be efficiently controlled to finally obtain new types of long-life, high-power, and energy-dense electrochemical power sources designed for meeting important technological and social demands, which span from the fast developing consumer electronic market to the renewal of energy economy and the control of the environmental conditions.

6. CONCLUSIONS

The use of nanoporous membranes as templates constitutes an attractive and practical methodology for the preparation of a variety of nanomaterials characterized by high aspect ratio, such as nanowires and nanotubes of metals, metal oxides, salts, conducting polymers, and composites. These nanomaterials show peculiar and advantageous performances for many electrochemical applications which span from electroanalysis to electrochemical energy storage, from electrochemical biosensors to nanomedicine.

It is reasonable to think that such a membrane-based approach to the synthesis of nanomaterials will find wider and wider application, mainly thanks to the fact that it allows the easy preparation and the rapid screening of the properties of new nanomaterials. For electroanalytical applications,

nanoelectrode ensembles show dramatically enhanced signal to background ratios with respect to any other electrode system, together with the possibility to measure rather easily the very fast charge transfer kinetic constant of interest for fundamental studies in electrochemical mechanisms. Combination of membrane-templated nanostructures of conducting polymers with biomolecules opens new perspectives in biosensing and nanomedicine, while the development of templated nanostructured electrodes for battery applications can help in overcoming some of the limits of conventional electrochemical energy storage systems.

The template synthesis makes the preparation of electrode systems with critical dimensions in the domain of nanometer accessible to almost any electrochemical laboratory; the next technological frontier will be developing methods and materials able to warranty full control of the size, spatial distribution, and addressability even of single nanoelectrode elements.

REFERENCES

1. H. Bracht, S. P. Nichols, W. Walukiewicz, J. P. Silveira, F. Briones, and E. E. Haller, *Nature* 408, 67 (2000).
2. P. Ugo, L. M. Moretto, S. Bellomi, V. P. Menon, and C. R. Martin, *Anal. Chem.* 68, 4169 (1996).
3. A. Malinauskas, *Synth. Met.* 107, 75 (1999).
4. R. Gref, Y. Minamitake, M. T. Peracchia, V. Trubetskoy, V. Torchilin, and R. Langer, *Science* 263, 1600 (1994).
5. R. M. Penner and C. R. Martin, *Anal. Chem.* 59, 2625 (1987).
6. I. F. Cheng and C. R. Martin, *Anal. Chem.* 60, 2163 (1988).
7. K. Uosaki, K. Okazaki, H. Kita, and H. Takahashi, *Anal. Chem.* 62, 652 (1990).
8. P. Ugo, in "Encyclopedia of Sensors" (C. A. Grimes, E. C. Dickey, and M. V. Pishko Eds.), Vol. 8, p. 67. American Scientific Publishers, Stevenson Ranch, CA, USA, 2006.
9. C. R. Martin and D. T. Mitchell, in "Electroanalytical Chemistry, a Series of Advances" (A. J. Bard and I. Rubinstein, Eds.), Vol. 21, p. 1. Marcel Dekker, New York, 1999.
10. L. F. Nazar, G. Goward, F. Leroux, M. Duncan, H. Huang, T. Kerr, and J. Gaubicher, *Int. J. Inorg. Mater.* 3, 191 (2001).
11. M. Hirshes, *Mater. Sci. Eng. B* B-108, 1 (2004).
12. V. P. Menon and C. R. Martin, *Anal. Chem.* 67, 1920 (1995).
13. E. Sabatani and J. Rubinstein, *J. Phys. Chem.* 91, 6663 (1987).
14. O. Chailapakul, L. Sun, C. J. Xu, and R. M. Crooks, *J. Am. Chem. Soc.* 115, 12459 (1993).
15. G. L. Che and C. R. Cabrera, *J. Electroanal. Chem.* 417, 155 (1996).
16. W. S. Baker and R. M. Crooks, *J. Phys. Chem. B* 102, 10041 (1998).
17. E. Jeonng, T. H. Galow, J. Schotter, M. Bal, A. Ursache, M. T. Tuominen, C. M. Stafford, T. P. Russel, and V. M. Rotello, *Langmuir* 17, 6396 (2001).
18. W. Cheng, S. Dong, and E. Wang, *Anal. Chem.* 74, 3599 (2002).
19. T. Liu, C. Burger, and B. Chu, *Pro. Polym. Sci.* 28, 5 (2003).
20. D. W. M. Arrigan, *Analyst* 129, 1157 (2004).
21. J. C. Hulteen and C. R. Martin, *J. Mater. Chem.* 7, 1075 (1997).
22. G. E. Possin, *Rev. Sci. Instrum.* 41, 772 (1970).
23. W. D. Williams and N. Giordano, *Rev. Sci. Instrum.* 55, 410 (1984).
24. P. Scopece, Ph.D. Thesis, University of Venice, Italy (2004).
25. P. Scopece, L. A. Baker, P. Ugo, and C. R. Martin, *Nanotechnology* 17, 3951 (2006).
26. B. B. Lakshmi, C. J. Patrissi, and C. R. Martin, *Chem. Mater.* 9, 2544 (1997).
27. C. J. Patrissi and C. R. Martin, *J. Electrochem. Soc.* 146, 3176 (1999).
28. N. Li, C. R. Martin, and B. Scrosati, *J. Power Sources* 97–98, 240 (2001).
29. G. Che, K. B. Jirage, E. R. Fisher, C. R. Martin, and H. Yoneyama, *J. Electrochem. Soc.* 144, 4296 (1997).
30. J. W. Diggle, T. C. Downie, and C. W. Goulding, *Chem. Rev.* 69, 365 (1969).
31. A. Despic, and V. P. Parkhutik, in "Modern Aspects of Electrochemistry" (J. O'M. Bockris, R. E. White, and B. E. Conway, Eds.), Vol. 20, p. 401. Plenum Press, New York, 1989.
32. P. Apel, *Radiat. Meas.* 34, 559 (2001).
33. Z. Siwy and A. Fulinski, *Phys. Rev. Lett.* 89, 198103 (2002).
34. Z. Siwy, D. Dobrev, R. Neumann, C. Trautmann, and K. Voss, *Appl. Phys. A* 76, 781 (2003).
35. N. Li, S. Yun, C. C. Harrell, and C. R. Martin, *Anal. Chem.* 76, 2025 (2004).
36. L. D.-D. Pra, E. Ferain, R. Legras, and S. Demoustier-Champagne, *Nucl. Instrum. Meth. Phys. Res. B* 196, 81 (2002).
37. P. Ugo, L. M. Moretto, G. A. Mazzocchin, P. Guerriero, and C. R. Martin, *Electroanalysis* 10, 1168 (1998).
38. A. T. Shawaqfeh and R. E. Baltus, *J. Membr. Sci.* 157, 147 (1999).
39. G. L. Hornyak, C. J. Patrissi, and C. R. Martin, *J. Phys. Chem. B* 101, 1548 (1997).
40. G. Patermarakis, *J. Electroanal. Chem.* 404, 69 (1996).
41. R. C. Furneaux, W. R. Rigby, and A. P. Davidsons, Porous films and methods forming them, USA, Patent number 4.687.551 (1987).
42. P. Bocchetta, C. Sunseri, A. Bottino, G. Capannelli, G. Chiavarotti, S. Piazza, and F. D. Quarto, *J. Appl. Electrochem.* 32, 977 (2002).
43. J. C. A. Foss, G. L. Hornyak, J. A. Stockert, and C. R. Martin, *J. Phys. Chem.* 98, 2963 (1994).
44. Z. Zhang, D. Gekhtman, M. S. Dresselhaus, and J. Y. Ying, *Chem. Mater* 11, 1659 (1999).
45. T. Parpaleis, J. M. Laval, M. Majda, and C. Bourdillon, *Anal. Chem.* 64, 641 (1992).
46. C. J. Miller and M. Majda, *J. Electroanal. Chem.* 207, 49 (1986).
47. M. Tian, S. Xu, J. Wang, N. Kumar, E. Wertz, Q. Li, P. M. Campbell, M. H. W. Chan, and T. E. Mallouk, *Nano Lett.* 5, 697 (2005).
48. R. L. Fleisher, P. B. Price, and R. M. Walker, in "Nuclear Tracks In Solids, Principle and Applications." Berkley, CA, 1975.
49. R. Spohr, Methods and device to generate a predetermined number of ion tracks. Germany, Patent number DE 2951376C2 (1983).
50. P. Y. Apel, Y. E. Korchev, Z. Siwy, R. Spohr, and M. Yoshida, *Nucl. Inst. Meth. Phys. Res. B* 184, 337 (2001).
51. C. A. Foss, Jr., in "Metal Nanoparticles, Synthesis, Characterization and Applications" (D. L. Feldheim and J. C. A. Foss, Eds.), Chap. 5. Marcel Dekker, New York, 2002.
52. C. Schönenberger, B. M. I. v. d. Zande, L. G. J. Fokkink, M. Henny, C. Schmid, M. Krüger, A. Bachtold, R. Huber, H. Birk, and U. Staufer, *J. Phys. Chem. B* 101, 5497 (1997).
53. T. M. Whitney, J. S. Jiang, P. C. Searson, and C. L. Chien, *Science* 261, 1316 (1993).
54. C. J. Brumlik and C. R. Martin, *Anal. Chem.* 64, 1201 (1992).
55. B. M. I. v. d. Zande, M. R. Böhmer, L. G. J. Fokkink, and C. Schönenbergher, *Langmuir* 16, 451 (2000).
56. X. Y. Zhang, L. D. Zhang, Y. Lei, L. X. Zhao, and Y. Q. Mao, *J. Mater. Chem.* 11, 1732 (2001).
57. L. Piraux, S. Dubois, and S. D. Champagne, *Nucl. Inst. Meth. Phys. Res. B* 131, 357 (1997).
58. H. Chiriac, A. E. Moga, M. Urse, and T.-A. Óvári, *Sens. Actuators, A* 106, 348 (2003).
59. J. Verbeeck, O. I. Lebedev, G. V. Tendeloo, L. Cagnon, C. Bougerol, and G. Tourillon, *J. Electrochem. Soc.* 150, E468 (2003).
60. K. R. Pirota, D. Navas, M. Hernández-Vélez, K. Nielsch, and M. Vásquez, *J. Alloys Compounds* 369, 18 (2004).
61. Y. Konishi, M. Motoyama, H. Matsushima, Y. Fukunata, R. Ishii, and Y. Ito, *J. Electroanal. Chem.* 559, 149 (2003).

62. M. Platt, R. A. W. Dryfe, and E. P. L. Roberts, *Electrochim. Acta* 49, 3937 (2004).
63. S. A. Sapp, B. Lakshmi, and C. R. Martin, *Adv. Mater.* 11, 402 (1999).
64. A. L. Prieto, M. S. Sander, M. S. M. González, R. Gronsky, T. Sands, and A. M. Stacy, *J. Am. Chem. Soc.* 123, 7160 (2001).
65. D. Routkevitch, T. Bigioni, M. Moskovits, and J. M. Xu, *J. Phys. Chem.* 100, 14037 (1996).
66. M. Tian, J. Wang, J. Kurtz, T. E. Mallouk, and M. H. W. Chan, *Nano Lett.* 3, 919 (2003).
67. M. L. Tian, J. Wang, J. Snyder, J. Kurtz, Y .Liu, P. Schiffer, T. E. Mallouk, and M. H. W. Chan, *Appl. Phys. Lett.* 83, 1620 (2003).
68. J. Wang, M. Tian, T. E. Mallouk, and M. H. W. Chan, *J. Phys. Chem. B* 108, 841 (2004).
69. J. G. Wang, M. L. Tian, T. E. Mallouk, and M. H. W. Chan, *Nano Lett.* 4, 1313 (2004).
70. J. Gu, J. Shi, L. Xiong, H. Chen, L. Li, and M. Ruan, *Solid State Sci.* 6, 747 (2004).
71. M. Wirtz and C. R. Martin, *Adv. Mater.* 15, 455 (2003).
72. K. B. Jirage, J. C. Hulteen, and C. R. Martin, *Anal. Chem.* 71, 4913 (1999).
73. K. B. Jirage, J. C. Hulteen, and C. R. Martin, *Science* 278, 655 (1997).
74. J. C. Hulteen, K. B. Jirage, and C. R. Martin, *J. Am. Chem. Soc.* 120, 6603 (1998).
75. J.-R. Ku, R. Vidu, R. Talroze, and P. Stroeve, *J. Am. Chem. Soc.* 126, 15 022 (2004).
76. B. Bercu, I. Enculescu, and R. Spohr, *Nucl. Instrum. Meth. B* 225, 497 (2004).
77. R. A. W. Dryfe, A. O. Simm, and B. Kralj, *J. Am. Chem. Soc.* 125, 13 014 (2003).
78. Y.-L. Tai and H. Teng, *Chem. Mater.* 16, 338 (2004).
79. H. X. He, J. S. Zhu, N. J. Tao, L. A. Nagahara, I. Amlani, and R. Tsui, *J. Am. Chem. Soc.* 123, 7730 (2001).
80. S. J. Choi and S. M. Park, *Adv. Mater.* 12, 1547 (2000).
81. L. Liang, J. Liu, C. F. Windish, G. J. Exarhos, and Y. H. Lin, *Angew. Chem. Ind. Ed.* 41, 3665 (2002)
82. T. Hatano, A. H. Bae, M. Takeuchi, N. Fujita, K. Kaneko, H. Ihara, M. Takafuji, and S. Shinkai, *Angew. Chem. Ind. Ed.* 43, 465 (2004).
83. C. Jérôme and R. Jérôme, *Angew. Chem. Ind. Ed.* 37, 2488 (1998).
84. A. D. W. Carswell, E. A. O'Rear, and B. P. Grady, *J. Am. Chem. Soc.* 125, 14 793 (2003).
85. C. R. Martin, *Science* 266, 1961 (1994).
86. Z. Cai and C. R. Martin, *J. Am. Chem. Soc.* 111, 4138 (1989).
87. J. He, W. Chen, N. Xu, L. Li, X. Li, and G. Xue, *Appl. Surf. Sci.* 221, 87 (2004).
88. W. Liang and C. R. Martin, *J. Am. Chem. Soc.* 112, 9666 (1990).
89. I. Tchepournaya, S. Vasilieva, S. Logvinov, A. Timonov, R. Amadelli, and D. Bartak, *Langmuir* 19, 9005 (2003).
90. A. Curulli, F. Valentini, S. Orlanducci, M. L. Terranova, and G. Palleschi, *Biosens. Bioelectron.* 20, 1223 (2004).
91. R. M. Hernandez, L. Richter, S. Semancik, S. Stranick, and T. E. Mallouk, *Chem. Mater.* 16, 3431 (2004).
92. J. Wang, J. Dai, and T. Yarlagadda, *Langmuir* 21, 9 (2005).
93. S. Demoustier-Champagne and P. Y. Stavaux, *Chem. Mater.* 11, 829 (1999).
94. G. Elie, G.G. Wallace, and T. Matsue, in "Handbook of Conducting Polymers." Marcel Dekker, New York, 1998.
95. X. Y. Cui, J. F. Hetke, J. A. Wiler, D. J. Anderson, and D. C. Martin, *Sens. Actuators A: Phys.* 93, 8 (2001).
96. J. Wang and M. Jiang, *Langmuir* 16, 2269 (2000).
97. S. Panero, G. Abbati, D. Renier, and V. Crescenti, PCT Int. Appl. WO 2003000309.S. (2003).
98. R. V. Parthasarathy and C. R. Martin, *Nature* 369, 298 (1994).
99. (a) P. Ugo, L. M. Moretto, and F. Vezzà, *ChemPhysChem* 3, 917 (2002); (b) P. Ugo, L. M. Moretto, and F. Vezzà, in "Sensors Update" (H. Baltes, G. K. Fedder, and J. G. Korvink, Eds.), Vol. 12, p. 121. Wiley-VCH, Weinheim, 2003.
100. C. Amatore, J. M. Saveant, and D. Tessier, *J. Electroanal. Chem.* 147, 39 (1983).
101. W. S. Baker and R. M. Crooks, *J. Phys. Chem. B* 102, 10 041 (1998).
102. L.M. Moretto, N. Pepe, and P. Ugo, *Talanta* 62, 1055 (2004).
103. H. J. Lee, C. Beriet, R. Ferrigno, and H. H. Girault, *J. Electroanal. Chem.* 502, 138 (2001).
104. J. C. Hulteen, V. P. Menon, and C. R. Martin, *J. Chem. Soc. Faraday Trans.* 92, 4029 (1996).
105. J. F. Cheng, L. D. Whiteley, and C. R. Martin, *Anal. Chem.* 61, 762 (1989).
106. B. Brunetti, P. Ugo, L. M. Moretto, and C. R. Martin, *J. Electroanal. Chem.* 491, 166 (2000).
107. P. Ugo and L. M. Moretto, *Electroanalysis* 7, 1105 (1995).
108. P. Ugo, N. Pepe, L. M. Moretto, and M. Battagliarin, *J. Electroanal. Chem.* 560, 51 (2003).
109. A. J. Bard and L. Faulkner, in "Electrochemical Methods" 2nd edn. Wiley, New York (2000).
110. B. A. Brookes, T. J. Davies, A. C. Fisher, R. G. Evans, S. J. Wilkins, K. Yunus, J. D. Wadhawan, and R. G. Compton, *J. Phys. Chem. B* 107, 1616 (2003).
111. T. J. Davies, B. A. Brookes, A. C. Fisher, K. Yunus, S. J. Wilkins, P. R. Green, J. D. Wadhawan, and R. G. Compton, *J. Phys. Chem. B* 107, 6431 (2003).
112. W. Cheng, S. Dong, and E. Wang, *Anal. Chem.* 74, 3599 (2002).
113. Y. Xian, M. Liu, Q. Cai, H. Li, J. Lu, and L. Jin, *Analyst* 126, 871 (2001).
114. M. Delvaux, S. Demoustier-Champagne, and A. Walcarius, *Electroanalysis* 16, 190 (2004).
115. Y. Lin, F. Lu, Y. Tu, and Z. Ren, *Nano Lett.* 4, 191 (2004).
116. E. Finot, E. Bourillot, R. Meunier-Prest, Y. Lacroute, G. Legay, M. Cherkaoui-Malki, N. Latruffe, O. Siri, P. Braunstein, and A. Dereux, *Ultramicroscopy* 97, 441 (2003).
117. J. Li, H. T. Ng, A. Cassell, W. Fan, H. Chen, Q. Ye, J. Koehne, J. Han, and M. Meyyappan, *Nano Lett.* 3, 597 (2003).
118. R. Gasparac, B. J. Taft, M. A. Lapierre-Devlin, A. D. Lazareck, J. M. Xu, and S. O. Kelly, *J. Am. Chem. Soc.* 126, 12 270 (2004).
119. B. Scrosati, *Nature* 373, 557 (1995).
120. W. Wakihara and O. Yamamoto, (Eds.), in "Lithium Ion Batteries-Fundamentals and Performance." Kodansha-Wiley-VCH, Wenheim, 1998.
121. W. van Schalkwijk .and B. Scrosati, (Eds.), in "Advances in Lithium-Ion Batteries." Kluwer Academic/Plenum Publishers, New York, 2002.
122. J.-M. Tarascon and M. Armand, *Nature* 414, 359 (2001).
123. S. Panero, B. Scrosati, M. Wachtler, and F. Croce, *J. Power Sources* 129, 90 (2004).
124. A. S. Aricò, P. Bruce, B. Scrosati, J.-M. Tarascon, and W. Van Schalkwijk, *Nature Mater.* 4, 366 (2005).
125. R. A. Huggins, in "Handbook of Battery Materials" (J. O. Besenhard, Ed.), Part III, Chap. 4. Wiley-VCH, Wenheim, 1999.
126. M. Winter and J. O. Besenhard, *Electrochim. Acta* 45, 31 (1999).
127. L. F. Nazar and O. Crosnier, in "Lithium Batteries Science and Technology" (G.-A. Nazri and G. Pistoia, Eds.). Kluwer Academic Publishers, 2004.
128. J. Yang, M. Winter, and J. O. Besenhard, *Solid State Ionics* 90, 281 (1996).
129. P. Poizot, S. Laurelle, S. Grugeon, L. Dupont, and J.-M. Tarascon, *Nature* 407, 496 (2000).
130. J. Graetz, C. C. Ahn, R. Yazami, and B. Fultz, *Electrochem. Solid-State Lett.* 6, A194 (2003).

131. H. Ikeda, M. Fujimoto, S. Fujitani, Y. Domoto, H. Yagi, H. Traui, N. Tamura, R. Ohshita, M. Kamino, and I. Yonezu, "The 42nd Battery Symposium in Japan." Yokohama, Japan (2001), p. 282.
132. M. Green, E. Fielder, B. Scrosati, M. Wachtler, and J. Serra Moreno, *Electrochem. Solid-State Lett.* 6, A75 (2003).
133. Y. Idota, T. Kubota, A. Matsufuji, Y. Maekawa, and T. Miyasaka, *Science* 276, 1395 (1997).
134. I. A. Courtney and J. R. Dahn, *J. Electrochem. Soc.* 144, 2045 (1997).
135. T. Brousse, S. M. Lee, L. Pasquerau, D. Deffves, and D. M. Schleich, *Solid State Ionics* 113–115, 51 (1998).
136. N. Li, C. R. Martin, and B. Scrosati, *J. Power Sources* 97–98, 240 (2001).
137. J.-M. Tarascon, S. Grugeon, S. Laruelle, D. Larcher, and P. Poizot, in "Lithium Batteries. Science and Technology" (G.-A. Nazri and G. Pistoia, Eds.), p. 220. Kluwer Academic Publications, Boston, 2004.
138. S. Denis, E. Baudrin, M. Touboul and J.-M. Tarascon, *J. Electrochem. Soc.* 144, 4099 (1997).
139. A. K. Padhi, K. S. Nanjundaswamy, and J. B. Goodenough, *J. Electrochem. Soc.* 144, 1188 (1997).
140. N. Ravet, Y. Chouninard, J. F. Magnan, S. Besner, M. Gauthier, and M. Armand, *J. Power Sources* 97–98, 503 (2001).
141. H. Huang, S.-C. Yin, and L. Nazar, *Electrochem. Solid-State Lett.* 4, 170 (2001).
142. G. Arnold, J. Garche, R. Hemmer, S. Strobele, C. Vogler, and M. Wohlfahrt-Meherens, *J. Power Sources* 119–121, 247 (2003).
143. F. Croce, A. D'Epifanio, J. Hassoun, and B. Scrosati, *Electrochem. Solid-State Lett.* 5, A47 (2002).
144. C. R. Sides, F. Croce, V. Y. Young, C. R. Martin, and B. Scrosati, *Electrochem. Solid-State Lett.* 8, A484 (2005).
145. F. Croce, G. B. Appetecchi, L. Persi, and B. Scrosati, *Nature* 394, 456 (1998).
146. F. Croce, R. Curini, A. Martinelli, L. Persi, F. Ronci, B. Scrosati, and R. Caminiti, *J. Phys. Chem.* 103, 10632 (1999).
147. F. Croce, L. Persi, B. Scrosati, F. Serraino-Fiory, E. Plichta, and M. A. Hendrickson, *Electrochim. Acta* 46, 2457 (2001).
148. D. R. MacFarlane, P. J. Newman, K. M. Nairn, and M. Forsyth, *Electrochim. Acta* 4, 1333 (1998).
149. H. Y. Sun, Y. Takeda, N. Imanishi, O. Yamamoto, and H.-J. Sohn, *J. Electrochem. Soc.* 147, 2462 (2000).
150. M. A. K. L. Dissanayake, P. A. R. D. Jayathilaka, R. S. P. Bokalawala, I. Albinsson, and B.-E. Mellander, *J. Power Sources* 119–121, 409 (2003).
151. J. Maier, *Prog. Solid. State Chem.* 23, 171 (1995).
152. G. B. Appetecchi, F. Croce, L. Persi, F. Ronci, and B. S. Crosati, *Electrochim. Acta* 45, 1481 (2000).
153. B. Kumar, S. J. Rodrigues, and L. Scanlon, *J. Electrochem. Soc.* 148, A1191 (2001).